Unknown Input Observer-Based Series DC Arc Fault Detection in DC Microgrids

Xiu Yao, *Member, IEEE*, Vu Le, *Student Member, IEEE*, and Inhwan Lee, *Member, IEEE*

***Abstract*—In this article, a fault detection and isolation technique for series arc faults in dc microgrids with multiple power electronics loads is proposed using unknown input observers (UIOs). The dc microgrid is first modeled as a linear system using its corresponding graph information, including the oriented incidence matrix. The lines are assumed to be in Pi form (resistive, inductive, and capacitive) defining the dynamic states: line currents and node voltages. Sources and loads are considered inputs to the network and details are presented to include the case where these are not measured. DC series arc faults are then analyzed as disturbances affecting any line. An UIO framework is then presented to detect and identify the faulted line using the network model. Simulation and experimental results are then presented.**

***Index Terms*—Fault detection, observers, microgrids.**

I. Introduction

DC POWER networks are currently being deployed as distribution systems in applications such as data centers, electric vehicles, more electric aircraft, spacecraft, and others [1]–[7]. DC networks can be advantageous due to the reduced number of conversion stages needed and lower number of transmission lines, improving the overall efficiency and size requirements. However, series high impedance faults are one of the main challenges affecting their safe operation.

When a small air gap is present, a voltage potential as small as around 20 V could lead to an arc discharge across the gap. The arc discharge creates a plasma channel across the gap, characterized by high impedance and high temperature. Due to the high impedance, the fault current is much lower than overcurrent and short-circuit faults, and therefore, cannot trigger traditional protection devices, such as circuit breakers timely. The high temperature from the arc discharge can burn the peripheral circuits and cause fire hazards [8].

Specifically, when the arc fault is in series with the load, namely series arc fault (SAF), it is difficult to detect and localize due to the following reasons.

1) Without the natural zero crossing point experienced by ac systems, the dc arc fault is more likely to sustain and cause fire hazards.
2) Many of the ac arc detection techniques are based on harmonic contents [9], [10], zero sequence current [11], or transients during reignition [12], which are absent in dc systems.
3) Series dc arc faults, which are likely to occur due to loosen connections, wire aging, etc., have fault current levels even lower than the nominal current [13]–[15].
4) The extensive usage of power electronics interfaces, advanced controllers, and high bandwidth energy storage controllers can sometimes dampen the fault response and blind the protection [16], [17].

Therefore, dc arc fault detection is both a challenging and important task to achieve reliable dc power systems with power electronics converters.

Series dc arc fault detection techniques have primarily focused on the analysis of a single line fault. Detection methods include the development of features based on time domain [e.g., current difference and Hurst exponent) [18], frequency domain (e.g., fast Fourier transform (FFT)] [19], and time-frequency domain (e.g., short time Fourier transform (STFT), wavelet transform (WT), etc.) [20]. In recent years, these features have been utilized in machine learning classifiers to improve the detection accuracy [21], [22]. However, these existing SAF detection techniques are typically focused on one line with resistive loads, whereas modern dc microgrids are composed of multiple branches and mainly nonlinear constant power loads (CPLs) interfaced with power electronics converters, such as buck converter.

The detection of the dc arc fault in systems with resistive loads have been extensively studied [23]–[25], with the focus of exploring different sensing and fault signature (features). However, challenges rise when the SAF occur with high penetration of power electronics. It has been reported that the power electronics controllers affect fault response, and therefore, fault detection [26]. The noise of power electronics circuits could also mask over certain frequency-domain-based fault detection algorithms. Moreover, with multiple power electronics interfaced loads connected in parallel, arc noise traveling and crosstalk caused mistriggers could happen, even with UL licensed commercial fault detection [27]. The noise generated during an SAF has been shown to travel to adjacent lines [16], [26], [28], with the possibility of causing mistriggers in detectors. For this reason, recent research has been focused on the localization of the SAF, in terms of the faulted line, within a dc microgrid or large-scale PV system [29]–[31]. Parameter estimation techniques have been proposed in [28] and [32]–[35], to estimate the line parameters, in particular, line resistance or conductance, to

Manuscript received April 26, 2021; revised September 6, 2021; accepted November 6, 2021. Date of publication November 17, 2021; date of current version December 31, 2021. This work was supported by National Science Foundation under Grant ECCS 1809839. Recommended for publication by Associate Editor D. Dong. *(Corresponding author: Xiu Yao.)*

The authors are with the Department of Electrical Engineering, The State University of New York at Buffalo, Buffalo, NY 14260 USA (e-mail: xiuyao@buffalo.edu; vule@buffalo.edu; inhwanle@buffalo.edu).

Color versions of one or more figures in this article are available at https://doi.org/10.1109/TPEL.2021.3128642.

Digital Object Identifier 10.1109/TPEL.2021.3128642

determine not only when an SAF occurs but also the specific line affected.

Fault detection and identification (FDI) of faults can be generally achieved either through parameter estimation (as shown in the previous references), or model-based techniques. The latter, has not been thoroughly explored for the SAF detection, although they have been used to detect and identify faults in general power electronic systems. For example, in [36], an open-loop hybrid observer was developed to detect and identify faults in power-electronic-based microgrids. The detection was accomplished by analyzing residuals (error terms between observer estimates and measurements) and an inner product with L_2 norm for fault identification. The latter part is particularly important as a single fault can affect multiple elements of the residual vector, complicating the identification process. Furthermore, an open-loop observer implies the error during the normal operation may not decrease to zero as quickly as desired. In [37], a closed-loop Luenberger observer was designed for detecting and identifying open-circuit faults in dc/dc converters. While multiple faults are considered, the identification part similarly relies on mapping each fault using an inner product, complicating the identification step.

Unknown input observers (UIO) are a type of estimators designed to be insensitive to a certain fault or faults, and are well known and have been used extensively for FDI applications [38], [39]. Developing parallel UIOs can be used for FDI, significantly simplifying the identification step: A single residual will be insensitive to where the fault is occurring. The UIOs have been developed for FDI of wind turbines [40] and electric machines in power systems [41]. More recently, these types of observers have been used for cyber-attack detection and identification in dc microgrids [42].

In this article, UIOs are used for the FDI of series high impedance arc faults in dc microgrids. Our main contributions include the following:

1) developing a dynamic model of the dc microgrid using the graph theory, where insights can be gained regarding the network observability for the design of UIOs;
2) experimental results of series arc faults with multiple lines, demonstrating the noise propagation;
3) an UIO formulation for the FDI of series arc faults;
4) an $\mathcal{L}_2$ stability-based threshold design for the residuals of the UIOs.

The rest of this article is organized as follows. The dynamic dc microgrid model and the modeling of the series arc fault, along with experimental testing, are described in Section II. In Section III, an UIO formulation is presented for the detection of series arc faults. The simulation and experimental results are presented in Sections IV and V, respectively. Finally, Section VI concludes this article.

The following notation will be used throughout this article. For a vector $x \in \mathbb{R}^n$, its 2 norm is defined as $||x||_2 = \sqrt{x_1^2 + \cdots + x_n^2}$. The space of m piecewise-continuous bounded functions is denoted as $\mathcal{L}_\infty^m$, with norm $||u||_{\mathcal{L}_\infty} = \sup_{t\geq 0} ||u(t)||_2 < \infty$, for $u(t) \in \mathcal{L}_\infty^m$. The space of m square integrable functions is denoted as $\mathcal{L}_2^m$. For $u(t) \in \mathcal{L}_2^m$, its norm is defined as $||u||_{\mathcal{L}_2} = (\int_0^\infty u^T(t)u(t)dt)^{1/2} < \infty$. A similar definition can be used to define $\mathcal{L}_p^m$, for $1 \leq p < \infty$, as the set of piecewise continuous functions satisfying $||u||_{\mathcal{L}_p} = (\int_0^\infty ||u(t)||^p dt)^{1/p} < \infty$. The truncation of a function $u(t) : \mathbb{R} \to \mathbb{R}^m$ is defined as follows:

$$u_\tau(t) = \begin{cases} u(t), & 0 \leq t \leq \tau \\ 0, & t > \tau. \end{cases}$$

For a matrix $A \in \mathbb{R}^{n\times n}$, its set of eigenvalues is known as the spectrum of A, denoted as $\sigma(A) \subset \mathbb{C}$. A symmetric matrix $M \in R^{n\times n}$ is positive definite if for any nonzero $x \in \mathbb{R}^n$, it satisfies $x^T Mx > 0$ and is denoted as $M \succ 0$. Finally, the symbol $\triangleq$ is used to denote equality by definition.

II. DC Microgrid Dynamic Model

The dynamic equations that govern the internal behavior of dc microgrids will be derived in this section. We consider the lines to be resistive and inductive, as well as having capacitance at both ends, either due to the transmission line or the input or output capacitance of loads and sources.

A. State-Space Model Derivation

The dc microgrid can be considered as an undirected graph defined as $\mathcal{G} = \{\mathcal{N},\ \mathcal{E}\}$, where $\mathcal{N} = \{1, \ldots, N\}$ are the set of nodes and $\mathcal{E} \subset \mathcal{N} \times \mathcal{N}$ are the set of edges. Let $N = |\mathcal{N}|$ be the total number of buses in the network and $E = |\mathcal{E}|$ the number of lines. An element of the edges $(i,\ j) \in \mathcal{E}$ implies that there is a transmission line between node i and j. While for an undirected graph $(i,\ j) = (j,\ i)$, we will always refer to this line as $(i,\ j)$ where $i < j$ and define the line current direction from node i to j.

The states of the dc microgrid can be defined by the line currents, $I = (I_{(i,j)}, \ldots, I_{(p,\ q)})^T \in \mathbb{R}^E$, and the node voltages $V = (V_1, \ldots, V_N)^T \in \mathbb{R}^N$. The linear state-space model can be obtained by deriving the oriented incidence matrix, $\mathcal{I} \in \mathbb{R}^{N\times E}$, which defines the connections between the nodes and the edges. For example, for a line $(i,\ j) \in \mathcal{E}$, the ith row of $\mathcal{I}$ will have a 1 related to this edge and the jth row/node will have a -1 in the same column. Therefore, each column of an oriented incidence matrix will add to zero. For each line $(i,\ j) \in \mathcal{E}$, we will define an associated line resistance and inductance as $r_{(i,j)}$ and $L_{(i,j)}$, respectively. Similarly, each bus $i \in \mathcal{N}$ will have an associated capacitance and parallel resistance: C_i and R_i, respectively. The linear state-space model of the internal dynamics of a dc network can be obtained as

$$\begin{pmatrix} \dot{I} \\ \dot{V} \end{pmatrix} = \begin{pmatrix} \Gamma & \mathcal{I}_L^T \\ -\mathcal{I}_C & \Lambda \end{pmatrix} \begin{pmatrix} I \\ V \end{pmatrix} + \begin{pmatrix} 0 & 0 \\ B_{\mathrm{s}} & B_{\mathrm{l}} \end{pmatrix} \begin{pmatrix} I_{\mathrm{s}} \\ I_{\mathrm{l}} \end{pmatrix} \tag{1}$$

where $\Gamma = \mathrm{Diag}(-\frac{r_{(i,j)}}{L_{(i,j)}}, \ldots, -\frac{r_{(p,q)}}{L_{(p,q)}}) \in \mathbb{R}^{E\times E}$, $\Lambda = \mathrm{Diag}(-\frac{1}{R_1 C_1}, \ldots, -\frac{1}{R_N C_N}) \in \mathbb{R}^{N\times N}$, and $\mathcal{I}_L^T \in \mathbb{R}^{E\times N}$ and $-\mathcal{I}_C \in \mathbb{R}^{N\times E}$ are derived as follows:

$$\mathcal{I}_L^T \triangleq \mathbf{L}^{-1}\mathcal{I}^T \tag{2}$$

$$\mathcal{I}_C \triangleq \mathbf{C}^{-1}\mathcal{I} \tag{3}$$

where $\mathbf{L} \triangleq \mathrm{Diag}(L_{(i,j)}, \ldots, L_{(p,q)})$, $\mathbf{C} \triangleq \mathrm{Diag}(C_1, \ldots, C_N)$, and $\mathcal{I}$ is the incidence matrix described previously.

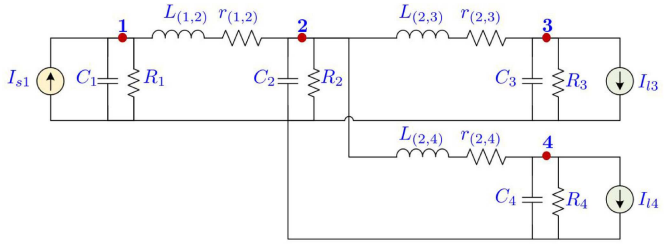

Fig. 1. Example of a four-bus dc network with detailed line parameters (Pi sections). Node 1 contains a source input and nodes 3 and 4 load inputs.

The inputs to the network are defined by the source currents $I_s \in \mathbb{R}^S$ where S is the number of sources and the load currents $I_l \in \mathbb{R}^L$ with L loads. The matrix $B_s \in \mathbb{R}^{N\times S}$ is associated with the source current inputs. If node $i \in \mathcal{N}$ has a source attached to it, its row would have a value of $\frac{1}{C_i}$ in the respective column. Similarly, the $B_l \in \mathbb{R}^{N\times L}$ would have an entry of $-\frac{1}{C_i}$ for a load attached to this node. The network model described by (1) will be referred to as the nominal or fault-free system and written for convenience as follows:

$$\begin{aligned} \dot{x} &= Ax + Bu \\ y &= Cx \end{aligned} \tag{4}$$

where $x = (I,\ V)^T \in \mathbb{R}^{E+N}, u = (I_s,\ I_l)^T \in \mathbb{R}^{S+L}$, and $y \in \mathbb{R}^p$ is a vector of the available sensors. The modeling presented in this section for the dc microgrid allows for fast computation and analysis of the internal dynamics of the network by using its associated graph $\mathcal{G} = \{\mathcal{N},\ \mathcal{E}\}$.

It is also possible to modify (1) to account for stiff voltage sources by deleting the respective node capacitance/state and if a certain source or load current is not measured, it can also be included as a state in the system defined by proper dynamics (e.g., an integrator). These specific cases will be explained in more detail in Section V.

B. Example for a Four-Bus System

As an example, consider the dc network shown in Fig. 1. The associated graph can be defined as $\mathcal{N} = \{1,\ 2,\ 3,\ 4\}$ and $\mathcal{E} = \{(1,\ 2),\ (2,\ 3),\ (2,\ 4)\}$. The oriented incidence matrix can be derived as follows:

$$\mathcal{I} = \begin{array}{c} \\ 1 \\ 2 \\ 3 \\ 4 \end{array} \begin{array}{c} \begin{array}{ccc} (1,2) & (2,3) & (2,4) \end{array} \\ \begin{pmatrix} 1 & 0 & 0 \\ -1 & 1 & 1 \\ 0 & -1 & 0 \\ 0 & 0 & -1 \end{pmatrix} \end{array}. \tag{5}$$

Therefore, the $\mathcal{I}_L^T$ matrix can be obtained as

$$\mathcal{I}_L^T = \begin{pmatrix} \frac{1}{L_{(1,2)}} & -\frac{1}{L_{(1,2)}} & 0 & 0 \\ 0 & \frac{1}{L_{(2,3)}} & -\frac{1}{L_{(2,3)}} & 0 \\ 0 & \frac{1}{L_{(2,4)}} & 0 & -\frac{1}{L_{(2,4)}} \end{pmatrix} \tag{6}$$

and the $\mathcal{I}_C$ matrix

$$\mathcal{I}_C = \begin{pmatrix} \frac{1}{C_1} & 0 & 0 \\ -\frac{1}{C_2} & \frac{1}{C_2} & \frac{1}{C_2} \\ 0 & -\frac{1}{C_3} & 0 \\ 0 & 0 & -\frac{1}{C_4} \end{pmatrix}. \tag{7}$$

The source and load current input matrices can be obtained as

$$B_s = \begin{pmatrix} \frac{1}{C_1} \\ 0 \\ 0 \\ 0 \end{pmatrix}, \quad B_l = \begin{pmatrix} 0 & 0 \\ 0 & 0 \\ -\frac{1}{C_3} & 0 \\ 0 & -\frac{1}{C_4} \end{pmatrix}. \tag{8}$$

Finally, $\Gamma = \text{Diag}(-\frac{r_{(1,2)}}{L_{(1,2)}}, -\frac{r_{(2,3)}}{L_{(2,3)}}, -\frac{r_{(2,4)}}{L_{(2,4)}})$ and $\Lambda = \text{Diag}(-\frac{1}{R_1C_1}, \ldots, -\frac{1}{R_4C_4})$. Using these matrices, the state-space model in (1) can be obtained.

C. Series Arc Fault in DC Microgrid

Series arc faults is a type of break in series with the line typically caused by loose connections or line degradation. As opposed to parallel faults, the line current does not generally increase or decrease significantly. The chaotic behavior of the fault introduces noise to the system that has been traditionally used for detection. However, this noise can propagate to adjacent lines and can cause possible mistriggers. In this subsection, we study experimentally the problem of arc noise in a dc network and formulate how this fault enters the system shown in (1).

1) Experimental Analysis: Using the hardware setup shown in Fig. 2(b), which will be used for the experimental result section, experiments were carried out with two CPLs in parallel. This type of configuration is common in modern distribution systems when one bus/node supplies power to multiple power electronics interfaced loads. The nominal test parameters of the setup are shown in Table I. Arc fault is created at the CPL1 branch, while CPL2 maintains normal operation.

The test results are shown in Fig. 3(a). After the arc fault was initiated at the CPL1 branch at approximate $t = 2.35$ s, its respective current has the following stages: initiation transient, controller response (due to CPLs), and steady-state arcing. Moreover, it can be seen that the CPL2 current and source current I_{dc} follow the general trend of the CPL1 current in terms of its high-frequency components, indicating the propagation of noise from CPL1.

In Fig. 3(b) and (c), the high-frequency components of I_{CPL2} and I_{dc} are almost as high as the faulted line current, I_{CPL1}, after the arc fault was initiated. In Fig. 3(b), the STFT of the three currents are shown. It can be seen that after $t = 2.35$ s, all of the three currents exhibit a similar pattern in terms of the amplitude at higher frequencies, appearing as if all three lines were faulted. In particular, the amplitude for the CPL1 current (faulted) and CPL2 (normal) is very similar. In Fig. 3(c), the variance of the wavelet coefficients for a frequency window of 25–37.5 kHz is shown. It can be seen that after the fault starts, all three line currents have an increase in this window. Therefore, detectors

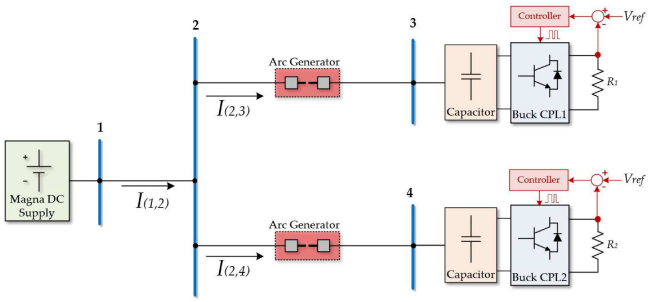

(a)

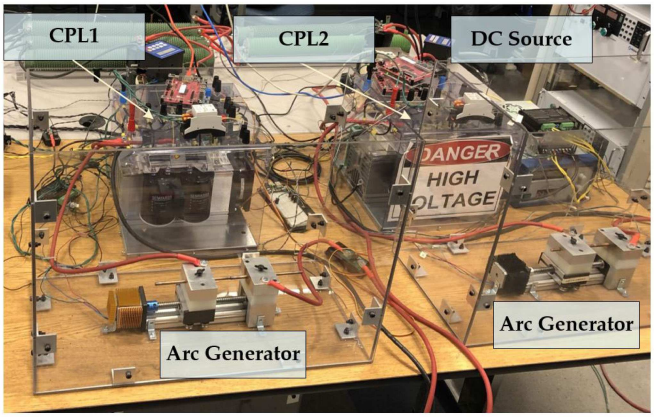

(b)

Fig. 2. Hardware setup for experimental results with four nodes. (a) High level diagram of experimental setup. (b) Experimental setup with two buck converter based CPLs.

TABLE I
TEST PARAMETERS WITH TWO CPLS

V_{dc}	270 V	I_{CPL1}	$[10-15]$ A
$V_{out(CPL1,CPL2)}$	200 V	I_{CPL2}	$[10-15]$ A

using the wavelet transform at each line can be triggered by this fault [20].

2) DC Network Model With Series Faults: In this section, we consider a common method for modeling series arc faults using a series resistance and voltage [43], shown in Fig. 4. The dynamic equation for the line current can be described using the KVL as follows:

$$\frac{d}{dt}I_{(i,j)} = -\frac{r_{(i,j)}}{L_{i,j}}I_{(i,j)} + \frac{1}{L_{i,j}}V_i - \frac{1}{L_{i,j}}V_j - \frac{1}{L_{i,j}}V_{f(i,j)} \tag{9}$$

where $V_{f(i,j)}$ is the overall voltage drop across the arc fault

$$V_{f(i,j)} = r_{f(i,j)}I_{(i,j)} + V_{\text{arc}(i,j)} \tag{10}$$

including the voltage drop over the resistive element and the voltage source. Therefore, it can be seen that the series arc fault is propagated to the microgrid dynamic model in (1) by the last term of (9), $-\frac{1}{L_{i,j}}V_{f(i,j)}$. Assuming that a series arc fault can occur at every line, the simplified dynamic model, (4), can be extended as

$$\begin{aligned} \dot{x} &= Ax + Bu + \sum_{(i,j)\in\mathcal{E}} B_{(i,j)}V_{f(i,j)} \\ y &= Cx \end{aligned} \tag{11}$$

where each $B_{(i,j)}$ is a column vector of zeros except for a $-\frac{1}{L_{(i,j)}}$ term in the same row as the respective line current/state $I_{(i,j)}$. The goal of the FDI system is to use the available measurements, y, and inputs, u, to detect the presence of a series arc fault, $V_{f(i,j)}$, and at the same time identify the faulted line.

III. UNKNOWN INPUT OBSERVER (UIO) BASED FAULT DETECTION AND LOCALIZATION

In recent years, model-based fault detection has gained significant attention in the detection and identification of faults in power-electronics-based systems [36], [37]. In these works, a Luenberger-type observer is typically used to estimate the states for the normal/fault free system (4). Once a fault occurs in the physical system, the observer error will increase and can be used for detection. However, the identification process can be slightly more difficult to achieve due to the need of postprocessing this error to select the right fault.

In this article, we consider a different type of observer, UIO, which can be properly designed to be insensitive to certain faults (error would still be zero), even during a fault. Therefore, multiple filters can be designed, each to be insensitive to different faults, simplifying both the detection and identification.

A. UIO Design

Consider the following simplified dc network model with a single line fault:

$$\begin{aligned} \dot{x} &= Ax + Bu + B_{(i,j)}V_{f(i,j)} \\ y &= Cx \end{aligned} \tag{12}$$

and assume that only the output vector, y, and the inputs, u, are available for the observer design. The UIO, insensitive to a series arc fault at line $(i,\ j) \in \mathcal{E}$, is defined as [39]

$$\begin{aligned} \dot{z}^{(i,j)} &= F^{(i,j)}z^{(i,j)} + T^{(i,j)}Bu + K^{(i,j)}y \\ \hat{x}^{(i,j)} &= z^{(i,j)} + H^{(i,j)}y \end{aligned} \tag{13}$$

where $\hat{x}^{(i,j)}$ are the estimated states (insensitive to a fault in line $(i,\ j) \in \mathcal{E}$) and $K^{(i,j)} = K_1^{(i,j)} + K_2^{(i,j)}$. Defining the error as $e^{(i,j)} \triangleq x - \hat{x}^{(i,j)}$, its dynamic behavior can be derived using (12) and (13) as

$$\begin{aligned} \dot{e}^{(i,j)} = &\left[A - H^{(i,j)}CA - K_1^{(i,j)}C\right]e^{(i,j)} \\ &+ \underbrace{\left[(A - H^{(i,j)}CA - K_1^{(i,j)}C) - F^{(i,j)}\right]}_{(17)}z^{(i,j)} \\ &+ \underbrace{\left[(A - H^{(i,j)}CA - K_1^{(i,j)}C)H^{(i,j)} - K_2^{(i,j)}\right]}_{(18)}y \end{aligned}$$

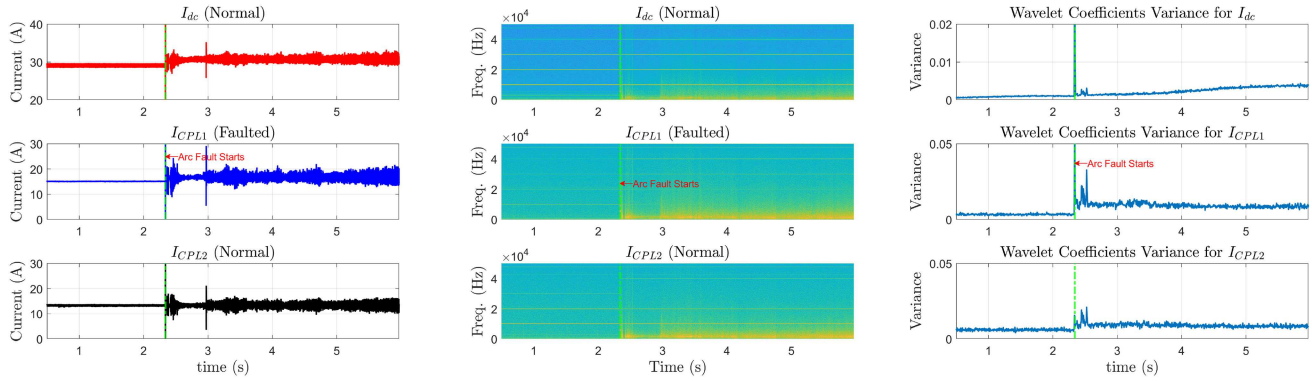

Fig. 3. Experimental results and analysis of series arc with multiple CPLs using the setup shown Fig. 2. (a) Line current waveforms. (b) Short time Fourier transform of currents. (c) Variance of wavelet coefficients. Frequency range: $[25, 37.5]$ kHz..

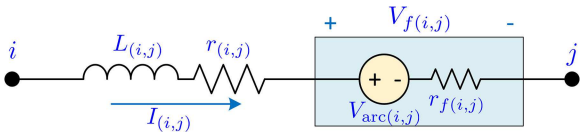

Fig. 4. Line formulation with a series arc fault model.

Algorithm 1: UIO Design for a Fault at Line $(i, j) \in \mathcal{E}$.

if rank$(CB_{(i,j)}) \neq$ rank$(B_{(i,j)})$ **then**
  UIO does not exist, STOP
end if
Solve $H^{(i,j)} = B_{(i,j)}[(CB_{(i,j)})^T(CB_{(i,j)})]^{-1}(CB_{(i,j)})^T$
Solve $T^{(i,j)} = I - H^{(i,j)}C$
Solve $A_1^{(i,j)} = T^{(i,j)}A$
if $(C,\ A_1^{(i,j)})$ is detectable **then**
  Design $K_1^{(i,j)}$ such that $\sigma(F^{(i,j)}) \subset \mathbb{C}^-$
end if
Solve $F^{(i,j)} = A_1^{(i,j)} - K_1^{(i,j)}C$
Solve $K_2^{(i,j)} = F^{(i,j)}H^{(i,j)}$
Solve $K^{(i,j)} = K_1^{(i,j)} + K_2^{(i,j)}$

$$+ \underbrace{\left[(I - H^{(i,j)}C) - T^{(i,j)}\right]}_{(16)} Bu(t)$$

$$+ \underbrace{(I - H^{(i,j)}C)B_{(i,j)}}_{(15)} V_{f(i,j)}. \tag{14}$$

Thus, it can be seen that if the following UIO conditions are satisfied [39]:

$$(H^{(i,j)}C - I)B_{(i,j)} = 0 \tag{15}$$

$$T^{(i,j)} = I - H^{(i,j)}C \tag{16}$$

$$F^{(i,j)} = A - H^{(i,j)}CA - K_1^{(i,j)}C \tag{17}$$

$$K_2^{(i,j)} = F^{(i,j)}H^{(i,j)} \tag{18}$$

where each equation is associated with the respective term in (14), the error dynamics are reduced to

$$\dot{e}^{(i,j)} = F^{(i,j)}e^{(i,j)}. \tag{19}$$

Furthermore, if $K_1^{(i,j)}$ is selected such that the eigenvalues of $F^{(i,j)}$ have negative real part, i.e., $\sigma(F^{(i,j)}) \subset \mathbb{C}^-$, the error will decay to 0 as $t \to \infty$. Such as $K_1^{(i,j)}$ matrix exists if and only if the pair $(C,\ A_1^{(i,j)})$ is detectable, where

$$A_1^{(i,j)} \triangleq A - H^{(i,j)}CA = T^{(i,j)}A. \tag{20}$$

The UIO satisfying (15)–(18) will be insensitive to an SAF in line (i, j), i.e., even after a fault occurs, the observer estimates will still converge to the states. The residual, insensitive to a fault at line $(i,\ j)$, is defined as

$$r^{(i,\,j)} \triangleq Ce^{(i,j)} = y - C\hat{x}^{(i,j)} = (I - CH^{(i,j)})y - Cz^{(i,j)} \tag{21}$$

and will be used in the next section to distinguish residuals associated with multiple faults at different lines. An algorithm describing the design of an UIO sensitive to a specific fault at line $(i, j) \in \mathcal{E}$ is shown in Algorithm 1, similar to the one presented in [39]. Notice the first condition, rank$(CB_{(i,j)}) \neq$ rank$(B_{(i,j)})$ is necessary in order to be able to solve for $H_{(i,j)}$ from (15). Using the network model in (1) and (11), we can state the following proposition.

Proposition 1: The UIO condition in (15) is not satisfied, and hence, an UIO does not exist for a fault at line (i, j), if the measurement vector, y, does not include the line current $I_{(i,j)}$.

Proof: It is assumed, although not explicitly stated, the measurement vector y, is a subset of the state vector x. Therefore, $y = Cx$ implies that C is a matrix such that each row contains a one in the column associated with the measured state, all other elements of each row are zero. Furthermore, the fault vector $B_{(i,j)}$ is nonzero only in the location of the state $I_{(i,j)}$. Therefore, if y does not include $I_{(i,j)}$, the column of C associated with state

Algorithm 2: Fault Detection and Identification Algorithm.

```
Obtain residuals for all lines
∀(i, j) ∈ E, ||r^(i,j)||_2^2 = r^(i,j)T r^(i,j)
if ∃||r^(i,j)||_2^2 > T then
    A fault has occurred
    if ∃||r^(p,q)||_2^2 < T then
        Fault occurred in line (p, q)
    end if
end if
```

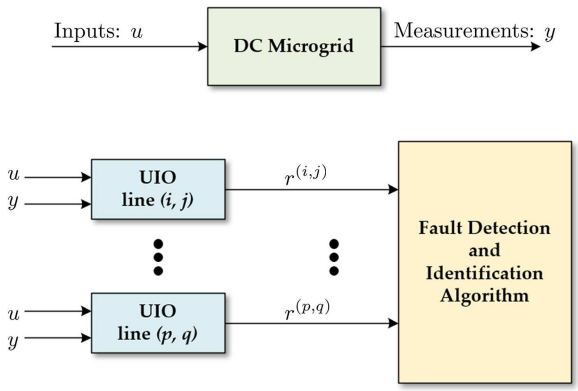

Fig. 5. Example of the UIO algorithm for residual generation and series arc FDI.

$I_{(i,j)}$ is all zeros, for which the following can be derived:

$$CB_{(i,j)} = 0 \;\Rightarrow\; (H^{(i,j)}C - I)B_{(i,j)} = -B_{(i,j)} \neq 0 \quad (22)$$

and the condition (15) is not satisfied. ■

B. Fault Detection and Identification

Let the microgrid be modeled as in (11), where a fault can occur at any edge/line $e \triangleq (i,\ j) \in \mathcal{E}$, multiple UIOs, each insensitive to a single line arc fault, can then be designed to detect and identify these faults. For example, if a series arc fault occurs at a specific line $(i,\ j) \in \mathcal{E}$, then the residuals for each UIO line will satisfy the following:

$$||r^{(i,\ j)}||_2^2 < T \quad (23)$$

$$||r^{(p,\ q)}||_2^2 \geq T \quad \forall\ (p,\ q) \neq (i,\ j) \in \mathcal{E} \quad (24)$$

where $T > 0$ is an appropriate threshold. Therefore, when a fault occurs at (i, j), the residual associated with the UIO at this line, $r^{(i,j)}$, will be insensitive to its fault, i.e., stay close to 0. However, the residuals for all other lines will increase, which can be shown by examining the error dynamics of all $(p,\ q) \neq (i,\ j) \in \mathcal{E}$ as

$$\dot{e}^{(p,q)} = F^{(p,q)}e^{(p,q)} + (H^{(p,q)}C - I)B_{(i,j)}V_{f(i,j)} \quad (25)$$

since

$$(H^{(p,q)}C - I)B_{(i,j)} \neq 0 \ \ \forall (p,q) \neq (i,j) \in \mathcal{E}. \quad (26)$$

A diagram showing the overall FDI scheme is shown in Fig. 5. As can be seen in this figure, an UIO will be designed to be insensitive to each line in the network using Algorithm 1. In addition, each UIO requires knowledge of the input vector, u, and the measurements, y. The final detection and isolation algorithm requires the analysis of the residuals and is shown in Algorithm 2. It can be seen that once the two-norm square of at least one residual crosses a threshold, a fault flag is raised. If the fault is associated with series arc in a line, $E - 1$ residuals will cross the threshold, where E is the number of lines. The only residual staying close to zero will determine the location of the fault, since it is designed to be insensitive to it.

C. Threshold Design

The threshold, T, in (23) plays a very important role in the UIO algorithm. A very high threshold may imply some norm squared of residuals will not cross it, whereas a small value may incur mistriggers. While the threshold can be designed using simulations, it is also possible to obtain analytical bounds. Towards this end, we can analyze how a series arc fault will affect the magnitude of the residuals.

Consider an UIO insensitive to a fault at line $(p, q) \in \mathcal{E}$ and assume a fault occurs at a different edge $(i, j) \neq (p, q) \in \mathcal{E}$. The error dynamics for this UIO can be modeled as a linear system of the form

$$\begin{aligned} \dot{e}^{(p,q)} &= F^{(p,q)}e^{(p,q)} + T^{(p,q)}B_{(i,j)}V_{f(i,j)} \\ r^{(p,q)} &= Ce^{(p,q)}. \end{aligned} \quad (27)$$

Assumption 1: A series arc fault at any line $(i, j) \in \mathcal{E}$ is bounded, i.e., $||V_{f(i,j)}(t)||_2 \leq \bar{V}_f\ \forall t \geq 0$.

Since $F^{(p,q)}$ is assumed to be Hurwitz (all eigenvalues have negative real part), a bounded fault $V_{f(i,j)}$ implies a bounded residual $r^{(p,q)}$ (bounded input bounded output) [44]. In particular, the concept of $\mathcal{L}_p$ or $\mathcal{L}_\infty$ stability can be used to determine the impact of faults to the residuals.

Definition 1: The error dynamics in (27) are finite gain $\mathcal{L}_p$ stable if $\exists \gamma_{(i,j)}^{(p,q)}, \beta \geq 0$ such that [44]

$$||r_\tau^{(p,q)}||_{\mathcal{L}_p} \leq \gamma_{(i,j)}^{(p,q)}||V_{f(i,j)-\tau}||_{\mathcal{L}_p} + \beta. \quad (28)$$

The parameter $\beta \geq 0$ is the bias and $\gamma_{(i,j)}^{(p,q)} \geq 0$ is known as the $\mathcal{L}_p$ gain of the system. Since $e(t) \to 0$ during normal operation, $\beta = 0$ [44]. The goal will be to select the smallest $\gamma_{(i,j)}^{(p,q)}$ for which (28) is satisfied for a fault at any line.

While an $\mathcal{L}_\infty$ bound provides a higher limit by which to guide the selection of T, the $\mathcal{L}_2$ stability/bounds can be used to obtain a root-mean-square-type bound for a truncated fault signal. Furthermore, this bound/parameter can be directly used as a threshold. We can consider the following semidefinite programming problem to obtain an optimal (least conservative) bound [45].

Proposition 2: For $(i, j) \neq (p, q) \in \mathcal{E}$, if there exists $\tilde{\gamma}_{(i,j)}^{(p,q)} > 0$ and $P \in \mathbb{R}^{n\times n}$ [n is the dimension of the error $e^{(p,q)}$ in (27)]

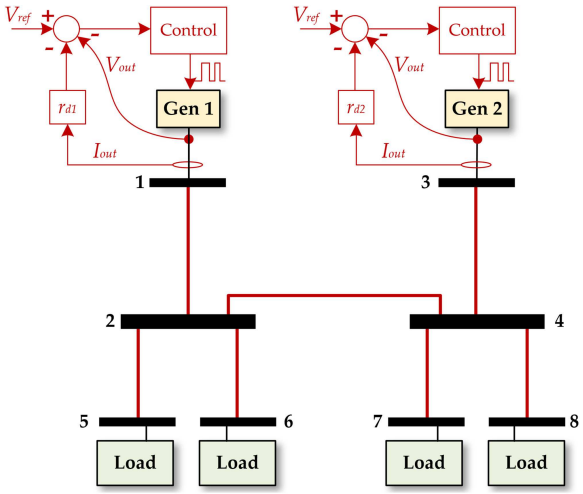

Fig. 6. DC network used for simulation results. The network has eight nodes and seven lines. Generators 1 and 2 are modeled using buck converters with droop control.

satisfying

$$\min_{\tilde{\gamma}^{(p,q)}_{(i,j)},\, P} \tilde{\gamma}^{(p,q)}_{(i,j)}$$
$$\text{subject to:}$$
$$P \succ 0$$
$$\begin{pmatrix} F^{(p,q)T}P + PF^{(p,q)} + C^T C & PT^{(p,q)}B_{(i,j)} \\ B^T_{(i,j)}T^{(p,q)T}P & -\tilde{\gamma}^{(p,q)}_{(i,j)} I \end{pmatrix} \preceq 0 \tag{29}$$

then $||r^{(p,q)}_\tau||_{\mathcal{L}_2} \leq \gamma^{(p,q)}_{(i,j)} ||V_{f(i,j)-\tau}||_{\mathcal{L}_2}$ for $\gamma^{(p,q)}_{(i,j)} = \sqrt{\tilde{\gamma}^{(p,q)}_{(i,j)}}$.

Proof: The proof is shown in the Appendix. ■

Therefore, for a fixed UIO insensitive to line $(p,\ q) \in \mathcal{E}$, the value $\gamma^{(p,q)}_{(i,j)}$ provides a way to understand how a series arc fault at a different line affects the residual term. A fault at certain lines may have a higher $\mathcal{L}_2$ gain than others. To ensure that the norm square of the residual can cross the threshold whenever there is a fault, we can select the threshold for the UIO at line (p, q) as follows:

$$T^{(p,q)} = \min_{(i,j)\neq(p,q)\in\mathcal{E}} \tilde{\gamma}^{(p,q)}_{(i,j)} ||V_{f-\tau}||^2_{\mathcal{L}_2} \tag{30}$$

where $\tilde{\gamma}^{(p,q)}_{(i,j)}$ is obtained using (29) and $||V_{f-\tau}||_{\mathcal{L}_2}$ is an estimate of the $\mathcal{L}_2$ norm of a typical series arc fault signature if known *a priori* (otherwise it can be used as a tuning parameter). Finally, one threshold can be selected for all UIOs as follows:

$$T = \min_{(p,q)\in\mathcal{E}} T^{(p,q)} \tag{31}$$

where $T^{(p,q)}$ is obtained from (30).

IV. Simulation Results

The system shown in Fig. 6 will be used for testing the proposed modeling and UIO design for series arc FDI. In this network, the set of nodes are $\mathcal{N} = \{1,\ 2, \ldots, 8\}$ and the set of edges are shown in red lines where an SAF can occur. The

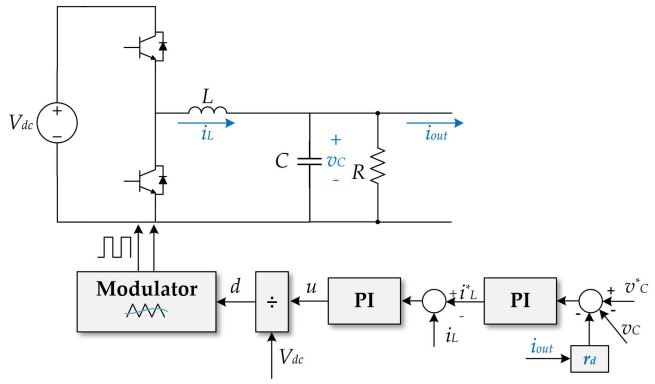

Fig. 7. Each source in the simulation model is composed of a buck converter with droop control.

TABLE II
Node and Line Parameters for the Simulation Model Shown in Fig. 6

Node	**1**	**2**	**3**	**4**	**5**	**6**	**7**	**8**
C_i (mF)	5	0.1	7	0.2	10	5	7	8
R_i (kΩ)	1	1	1	1	1	1	1	1
Edge	**(1, 2)**	**(2, 4)**	**(3, 4)**	**(2, 5)**	**(2, 6)**	**(4, 7)**	**(4, 8)**	
$r_{(i,j)}$ (mΩ)	10	1	10	5	4	6	7	
$L_{(i,j)}$ (mH)	0.1	0.05	0.2	0.075	0.075	0.075	0.075	

two sources, generators 1 and 2, are modeled using closed-loop controlled dc/dc converters (buck) with equal droop gains to ensure each generator supplies a similar amount of current, as shown in Fig. 7. The simulation and UIOs time step is $T_s = 1\ \mu$s. The four loads are simplified as constant current loads. The nominal dc bus voltage is 400 V. Each line is assumed to be resistive and inductive, while in each node, a capacitance with a parallel resistor is added. While the nodes with sources and loads attached typically have a output and input capacitance, respectively, the capacitor value at nodes 2 and 4 are assumed to be significantly smaller. The simulation parameters are shown in Table II.

A. Nominal Operation

During normal operation, the two generators attempt to provide a similar amount of power to the loads by using droop control. The load current at nodes 5–8 are 50, 70, 30, and 20 A, respectively. At time $t = 0.4$ s, the load at node 8 is changed from 20 to 50 A. The transient response of the voltage at every node and line currents is shown in Fig. 8. We can see that the current in line $(2,\ 4)$ is negative, implying that the generator 2 is sending current to supply the loads at nodes 5 and 6, and the line currents (1,2) and (3,4) are relatively similar due to the droop control. Furthermore, the norm of the residuals, $||r^{(i,j)}||^2_2 \ \ \forall (i,j) \in \mathcal{E}$, associated with the UIOs at each line, are shown in the bottom subfigure. It can be seen that a load change does not significantly alter the estimation error.

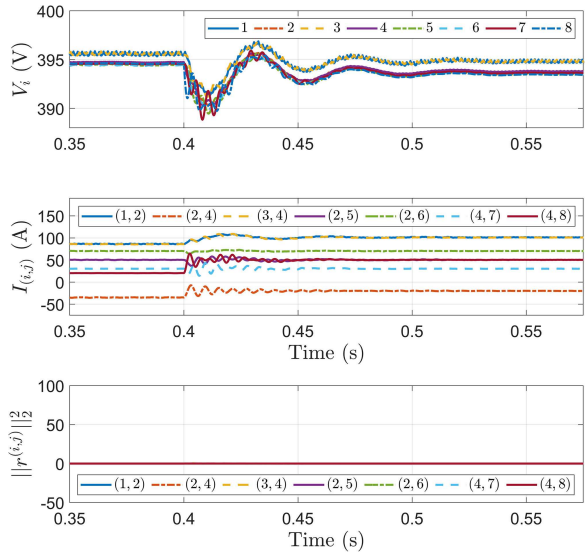

Fig. 8. Simulation results during a change in the load at node 8. (Top) Node voltages. (Middle) Line currents. (Bottom) Norm square of the UIO residuals.

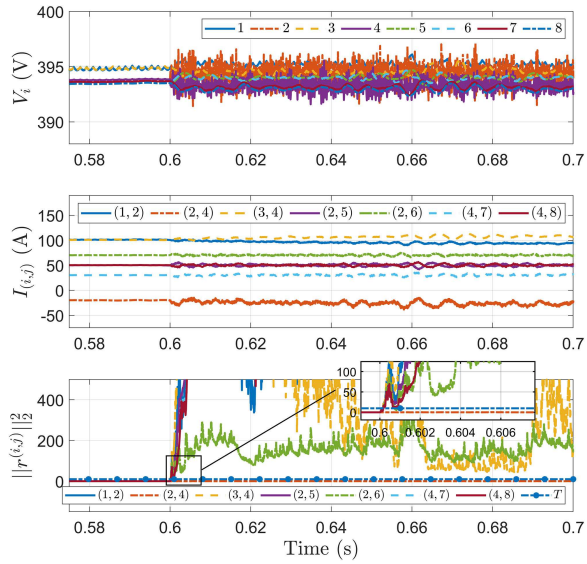

Fig. 9. Simulation results during a series arc fault in line (2,4). (Top) Node voltages. (Middle) Line currents. (Bottom) Threshold and norm square of the UIO residuals.

B. Fault in Line (2,4)

Using the same parameters as the nominal operation in the previous section, we now consider a series arc fault. For the design of the UIOs, we assume that the measurement vector contains the line currents at every line, and the voltage at nodes 1, 2, and 3 only. For this scenario, the UIOs can be designed at every line, although certain lines are only detectable (not observable).

The simulation results are shown in Fig. 9. At time $t = 0.6$ s, a series dc arc fault occurs in line (2,4). It can be seen how the voltages near the fault and the line currents, top and middle subfigures, respectively, are affected by a fault. Furthermore, it can be seen that all of the residual norms are affected by this fault with the exception of the residual insensitive to a fault in this line, (2,4), shown in dashed orange in the bottom subfigure. Therefore, Algorithm 2 can be used to detect the fault occurring at this line. Finally, the optimal threshold computed using (29)–(31) is $T = 9.9$ (assuming $||V_{f-\tau}||_{\mathcal{L}_2} = 1$) and is shown in Fig. 9 (bottom). It can be seen all of the residuals, except $||r_{(2,4)}||_2^2$, cross the threshold as desired.

V. Experimental Results

The UIO techniques are next tested on a four-node microgrid testbed shown in Fig. 2 with a discretization time step of $T_s = 5$ μs. The circuit diagram is shown in Fig. 2(a), while the experimental testbed is shown in Fig. 2(b). Two series arc fault generators are located in lines (2,3) and (2,4). For this reason, only two UIOs will be designed, each meant to be insensitive to an SAF at each of these lines. Node one is assumed to be a stiff voltage source and the load currents at nodes three and four are not measured. Therefore, the states and input become

$$x = \left(I_{(1,2)}\ I_{(2,3)}\ I_{(2,4)}\ V_2\ V_3\ V_4\ I_{l3}\ I_{l4}\right)^T \tag{32}$$

$$u = V_{s1} \tag{33}$$

where V_{s1} is the voltage source at node 1 and I_{l3} and I_{l4} are the load currents at nodes three and four, respectively. Since the load currents are generally constant, they will be generated by an integrator of the form

$$\dot{I}_{li} = 0, \quad i = 3,\ 4. \tag{34}$$

The same procedure to define the network dynamics shown in Section II can be followed, with the main exception of ignoring the node 1 voltage, which essentially eliminates the first row of the oriented incidence matrix, and adding the two load currents as states. The measured outputs are then

$$y = \left(I_{(2,3)}\ I_{(2,4)}\ V_3\ V_4\right)^T. \tag{35}$$

Using these outputs/measurements, the UIOs for both lines (2,3) and (2,4) are observable, implying that the UIOs' closed-loop eigenvalues can be placed at any desired location on the complex plane. Finally, the threshold is computed optimally using (29)–(31) and $||V_{f-\tau}||_{\mathcal{L}_2} = 50$ (obtained from experimental results).

A. Case 1: Intermittent Arcing

The experimental results with intermittent arcing are shown in Fig. 10. At time $t = 0.3$ s, a series arc fault occurs in line (2,3). The first plot shows the voltages at nodes 2, 3, and 4, represented by the blue, orange, and yellow traces, respectively. The middle plot shows the line currents $I_{(1,2)}$, $I_{(2,3)}$, and $I_{(2,4)}$ by the blue, orange, and yellow lines, respectively. It can be seen that while the SAF is intermittent, there are large current spikes. However, after approximately $t = 0.35$ s, the SAF becomes steady and it is difficult to differentiate the fault by simply analyzing the current waveforms. The last subfigure shows the two-norm square of the residuals for each line, $r^{(2,3)}$ and $r^{(2,4)}$, each meant to be insensitive to a fault at their respective lines. Therefore, when the arc fault occurs, the residual associated with line (2,4) increases. This fault can then be localized by identifying the

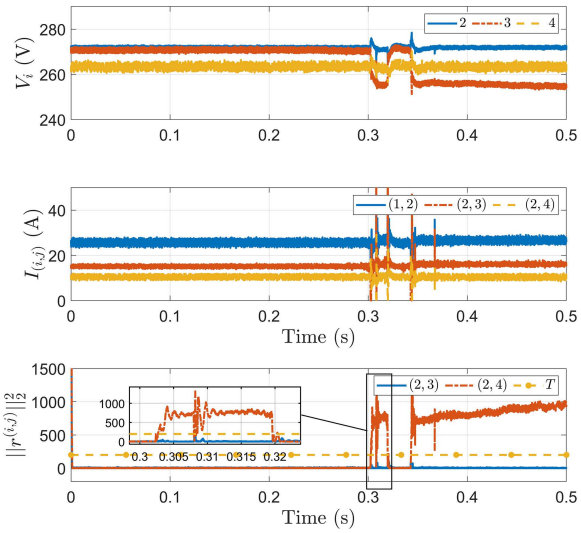

Fig. 10. Experimental results during an intermittent series arc fault in line (2,3). (Top) Node voltages. (Middle) Line currents. (Bottom) Threshold and norm square of the UIO residuals.

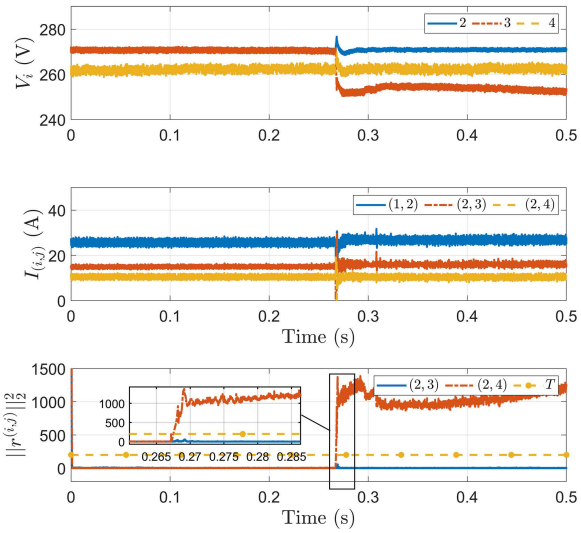

Fig. 11. Experimental results during a stable series arc fault in line (2,3). (Top) Node voltages. (Middle) Line currents. (Bottom) Threshold and norm square of the UIO residuals.

residual, which is not affected by the fault, in this case, $r^{(2,3)}$ remains very close to zero during the entire intermittent and steady-state arcing. In addition, it is possible to see how quickly the fault can be detected and identified, by the fast response of the residuals.

B. Case 2: Stable Arcing

The case where a series arc fault directly achieves steady-state arcing is also presented. The experimental results are shown in Fig. 11. At time $t = 0.27$ s, the series arc fault occurs on line (2,3) and remains stable throughout the duration of the experiment. In this case, the node voltages and line currents (top and middle subfigures) show significantly less oscillation during the fault. Examining the line residuals (bottom subfigure), it can be seen that the 2-norm squared of the UIO residual associated with line (2,4), $||r^{(2,4)}||_2^2$, increases significantly, marking the beginning of a fault. Finally, it is possible to conclude the fault occurs at line (2,3) as $||r^{(2,3)}||_2^2$ remains close to zero.

VI. Conclusion

This article presents an SAF detection and identification technique using UIOs. The internal dc network dynamics are first derived using the graph theory. The lines are assumed to be resistive and inductive while a capacitor is placed at each node. The states, therefore, include line currents and node voltages, which are then used to formulate an SAF event at any line. An UIO-based algorithm is then presented for FDI, by creating multiple observers, each insensitive to a single line fault.

Simulation results are then presented for a eight-bus network with seven lines. It is shown how the residuals can then be used to detect and localize the fault at a particular line. Experimental results are also shown for a four-bus dc network with three lines. In this case, the load currents are added as states to the system since they are not measured. Two cases are presented: intermittent and stable arcing. For both of these scenarios, the proposed algorithm is able to detect and identify the faulted line very quickly. Future work includes developing a systematic method to reduce the size of the UIOs, such as reduced-order and/or distributed/decentralized observers, and applying the proposed techniques to larger networks.

Appendix

A. Proof of Proposition 2

The proof is similar to [45, ch. 6.3.2] and can be derived for the system in (27) by considering a quadratic Lyapunov function as follows:

$$V\left(e^{(p,q)}\right) = e^{(p,q)T} P e^{(p,q)} > 0 \tag{36}$$

satisfying

$$\frac{d}{dt} V\left(e^{(p,q)}\right) + r^{(p,q)T} r^{(p,q)} - \gamma_{(i,j)}^{(p,q)^2} V_{f(i,j)-\tau}^T V_{f(i,j)-\tau} \leq 0 \tag{37}$$

where $r^{(p,q)} = Ce^{(p,q)}$. Equations (36) and (37) can be placed into linear matrix inequalities as shown in the constraints of (29), where $\tilde{\gamma}_{(i,j)}^{(p,q)} = \gamma_{(i,j)}^{(p,q)^2}$ to avoid the nonlinear term. If a solution to (29) exists, then the following holds:

$$V\left(e^{(p,q)}\right) + \int r^{(p,q)T} r^{(p,q)} dt - \gamma_{(i,j)}^{(p,q)^2} \int V_{f(i,j)-\tau}^T V_{f(i,j)-\tau} dt \leq 0 \tag{38}$$

by integrating both sides of (37). Since $V(e^{(p,q)}) > 0$, then

$$||r_\tau^{(p,q)}||_{\mathcal{L}_2}^2 - \gamma_{(i,j)}^{(p,q)^2} ||V_{f(i,j)-\tau}||_{\mathcal{L}_2}^2 \leq -V\left(e^{(p,q)}\right) < 0 \tag{39}$$

and we can obtain the desired result $||r_\tau^{(p,q)}||_{\mathcal{L}_2} \leq \gamma_{(i,j)}^{(p,q)} ||V_{f(i,j)-\tau}||_{\mathcal{L}_2}$. □

REFERENCES

[1] A. Pratt, P. Kumar, and T. V. Aldridge, "Evaluation of 400V DC distribution in telco and data centers to improve energy efficiency," in *Proc. 29th Int. Telecommun. Energy Conf.*, Sep. 2007, pp. 32–39.

[2] K. Emadi and M. Ehsani, "Aircraft power systems: Technology, state of the art, and future trends," *IEEE Aerosp. Electron. Syst. Mag.*, vol. 15, no. 1, pp. 28–32, Jan. 2000.

[3] D. Izquierdo, R. Azcona, F. J. L. d. Cerro, C. Fernández, and B. Delicado, "Electrical power distribution system (HV270DC), for application in more electric aircraft," in *Proc. 25th Annu. IEEE Appl. Power Electron. Conf. Expo.*, Feb. 2010, pp. 1300–1305.

[4] J. A. Weimer, "Electrical power technology for the more electric aircraft," in *Proc. 12th AIAA/IEEE Digit. Avionics Syst. Conf.*, Oct.1993, pp. 445–450.

[5] A. Emadi, S. S. Williamson, and A. Khaligh, "Power electronics intensive solutions for advanced electric, hybrid electric, and fuel cell vehicular power systems," *IEEE Trans. Power Electron.*, vol. 21, no. 3, pp. 567–577, May 2006.

[6] E. W. Gholdston, K. Karimi, F. C. Lee, J. Rajagopalan, Y. Panov, and B. Manners, "Stability of large DC power systems using switching converters, with application to the international space station," in *Proc. 31st Intersociety Energy Convers. Eng. Conf.*, Aug.1996, vol. 1, pp. 166–171.

[7] L. Herrera, W. Zhang, and J. Wang, "Stability analysis and controller design of DC microgrids with constant power loads," *IEEE Trans. Smart Grid*, vol. 8, no. 2, pp. 881–888, Mar. 2017.

[8] K. M. Armijo, J. Johnson, M. Hibbs, and A. Fresquez, "Characterizing fire danger from low-power photovoltaic arc-faults," in *Proc. IEEE 40th Photovolt. Specialist Conf.*, 2014, pp. 3384–3390.

[9] S.-J. Huang and C.-T. Hsieh, "High-impedance fault detection utilizing a Morlet wavelet transform approach," *IEEE Trans. Power Del.*, vol. 14, no. 4, pp. 1401–1410, Oct. 1999.

[10] A. Emanuel, D. Cyganski, J. Orr, S. Shiller, and E. Gulachenski, "High impedance fault arcing on sandy soil in 15 kV distribution feeders: Contributions to the evaluation of the low frequency spectrum," *IEEE Trans. Power Del.*, vol. 5, no. 2, pp. 676–686, Apr. 1990.

[11] J. T. A. Vianna, L. R. Araujo, and D. R. R. Penido, "High impedance fault area location in distribution systems based on current zero sequence component," *IEEE Latin Amer. Trans.*, vol. 14, no. 2, pp. 759–766, Feb. 2016.

[12] N. I. Elkalashy, "Modeling and detection of high impedance arcing fault in medium voltage networks," Ph.D. dissertation, Helsinki Univ. Technol., Espoo, Finland, 2007.

[13] J. Johnson *et al.*, "Photovoltaic DC ARC fault detector testing at Sandia National Laboratories," in *Proc. 37th IEEE Photovolt. Specialist Conf.*, Jun. 2011, pp. 3614–3619.

[14] M. Naidu, T. J. Schoepf, and S. Gopalakrishnan, "Arc fault detection scheme for 42-V automotive DC networks using current shunt," *IEEE Trans. Power Electron.*, vol. 21, no. 3, pp. 633–639, May 2006.

[15] J. A. Momoh, D. M. V. Kumar, A. S. Ishola-Salawu, R. Sowah, and R. Button, "Lab VIEW based implementation of remedial action for DC arcing faults in a spacecraft," in *Proc. Power Eng. Soc. General Meeting*, Jul. 2003, vol. 1, pp. 491–498.

[16] X. Yao, L. Herrera, and J. Wang, "Impact evaluation of series DC arc faults in DC microgrids," in *Proc. IEEE Appl. Power Electron. Conf. Expo.*, Mar. 2015, pp. 2953–2958.

[17] P. Rakhra, P. J. Norman, S. D. Fletcher, S. J. Galloway, and G. M. Burt, "Evaluation of the impact of high-bandwidth energy-storage systems on DC protection," *IEEE Trans. Power Del.*, vol. 31, no. 2, pp. 586–595, Apr. 2016.

[18] Y. Abdullah *et al.*, "Hurst-exponent-based detection of high-impedance DC Arc events for 48-V systems in vehicles," *IEEE Trans. Power Electron.*, vol. 36, no. 4, pp. 3803–3813, Apr. 2021.

[19] M. H. R. A. Syafiri, E. Prasetyono, M. K. Khafidli, D. O. Anggriawan, and A. Tjahjono, "Real time series DC arc fault detection based on fast Fourier transform," in *Proc. Int. Electron. Symp. Eng. Technol. Appl.*, 2018, pp. 25–30.

[20] X. Yao, L. Herrera, S. Ji, K. Zou, and J. Wang, "Characteristic study and time domain-discrete wavelet transform based hybrid detection of series DC Arc faults," *IEEE Trans. Power Electron.*, vol. 29, no. 6, pp. 3101–3115, Jun. 2014.

[21] V. Le, X. Yao, C. Miller, and B.-H. Tsao, "Series DC arc fault detection based on ensemble machine learning," *IEEE Trans. Power Electron.*, vol. 35, no. 8, pp. 7826–7839, Aug. 2020.

[22] R. D. Telford, S. Galloway, B. Stephen, and I. Elders, "Diagnosis of series DC arc faults—A machine learning approach," *IEEE Trans. Ind. Informat.*, vol. 13, no. 4, pp. 1598–1609, Aug. 2017.

[23] W. Miao, Q. Xu, K. H. Lam, P. W. T. Pong, and H. V. Poor, "DC arc-fault detection based on empirical mode decomposition of arc signatures and support vector machine," *IEEE Sensors J.*, vol. 21, no. 5, pp. 7024–7033, Mar. 2021.

[24] K. Xia *et al.*, "Wavelet entropy analysis and machine learning classification model of DC serial arc fault in electric vehicle power system," *IET Power Electron.*, vol. 12, no. 15, pp. 3998–4004, 2019.

[25] X. Yao, L. Herrera, S. Ji, K. Zou, and J. Wang, "Characteristic study and time-domain discrete-wavelet-transform based hybrid detection of series DC arc faults," *IEEE Trans. Power Electron.*, vol. 29, no. 6, pp. 3103–3115, Jun. 2014.

[26] X. Yao, "Study on DC arc faults in ring-bus DC microgrids with constant power loads," in *Proc. IEEE Energy Convers. Congr. Expo.*, 2016, pp. 1–5.

[27] J. Johnson, K. M. Armijo, M. Avrutsky, D. Eizips, and S. Kondrashov, "Arc-fault unwanted tripping survey with UL 1699B-listed products," in *Proc. IEEE 42nd Photovolt. Specialist Conf.*, 2015, pp. 1–6.

[28] K. Gajula and L. Herrera, "Detection and localization of series Arc faults in DC microgrids using Kalman filter," *IEEE Trans. Emerg. Sel. Topics Power Electron.*, vol. 9, no. 3, pp. 2589–2596, Jun. 2021.

[29] H.-P. Park, M. Kim, J. Jung, and S. Chae, "Series DC arc fault detection method for PV systems employing differential power processing structure," *IEEE Trans. Power Electron.*, vol. 36, no. 9, pp. 9787–9795, Sep. 2021.

[30] N. L. Georgijevic, M. V. Jankovic, S. Srdic, and Z. Radakovic, "The detection of series arc fault in photovoltaic systems based on the arc current entropy," *IEEE Trans. Power Electron.*, vol. 31, no. 8, pp. 5917–5930, Aug. 2016.

[31] M. K. Alam, F. Khan, J. Johnson, and J. Flicker, "A comprehensive review of catastrophic faults in PV arrays: Types, detection, and mitigation techniques," *IEEE J. Photovolt.*, vol. 5, no. 3, pp. 982–997, May 2015.

[32] K. Gajula, X. Yao, and L. Herrera, "Dual state - parameter estimation for series arc fault detection on a DC microgrid," in *Proc. IEEE Energy Convers. Congr. Expo.*, 2020, pp. 4649–4655.

[33] K. O'Shea, B.-H. Tsao, L. Herrera, and C. Miller, "Recursive least squares parameter estimation for DC fault detection and localization," in *Proc. IEEE Nat. Aerosp. Electron. Conf.*, 2019, pp. 7–10.

[34] K. K. Gajula, L. Herrera, and X. Yao, "Detection of series DC arc on a distribution node using discrete-time parameter identification techniques," in *Proc. IEEE Appl. Power Electron. Conf. Expo.*, 2019, pp. 3007–3012.

[35] L. Herrera and X. Yao, "Parameter identification approach to series DC arc fault detection and localization," in *Proc. IEEE Energy Convers. Congr. Expo.*, 2018, pp. 497–501.

[36] J. Poon, P. Jain, I. C. Konstantakopoulos, C. Spanos, S. K. Panda, and S. R. Sanders, "Model-based fault detection and identification for switching power converters," *IEEE Trans. Power Electron.*, vol. 32, no. 2, pp. 1419–1430, Feb. 2017.

[37] S. Zhuo, A. Gaillard, L. Xu, C. Liu, D. Paire, and F. Gao, "An observer-based switch open-circuit fault diagnosis of DC-DC converter for fuel cell application," *IEEE Trans. Ind. Appl.*, vol. 56, no. 3, pp. 3159–3167, May/Jun. 2020.

[38] J. Chen, R. J. Patton, and H.-Y. Zhang, "Design of unknown input observers and robust fault detection filters," *Int. J. Control*, vol. 63, no. 1, pp. 85–105, 1996.

[39] J. Chen and R. J. Patton, *Robust Model-Based Fault Diagnosis for Dynamic Systems*, vol. 3. Berlin, Germany: Springer, 2012.

[40] P. F. Odgaard and J. Stoustrup, "Unknown input observer based detection of sensor faults in a wind turbine," in *Proc. IEEE Int. Conf. Control Appl.*, 2010, pp. 310–315.

[41] H. H. Alhelou, "Fault detection and isolation in power systems using unknown input observer," in *Advanced Condition Monitoring and Fault Diagnosis of Electric Machines*. Pennsylvania, PA, USA: IGI Global, 2019, pp. 38–58.

[42] A. J. Gallo, M. S. Turan, F. Boem, T. Parisini, and G. Ferrari-Trecate, "A distributed cyber-attack detection scheme with application to DC microgrids," *IEEE Trans. Automat. Control*, vol. 65, no. 9, pp. 3800–3815, Sep. 2020.

[43] F. M. Uriarte *et al.*, "A DC arc model for series faults in low voltage microgrids," *IEEE Trans. Smart Grid*, vol. 3, no. 4, pp. 2063–2070, Dec. 2012.

[44] H. K. Khalil, *Nonlinear Systems*, 3rd ed. Upper Saddle River, NJ, USA: Prentice Hall, 2002.

[45] S. Boyd, L. El Ghaoui, E. Feron, and V. Balakrishnan, *Linear Matrix Inequalities in System and Control Theory*, Philadelphia, PA, USA: SIAM, 1994.

Xiu Yao (Member, IEEE) received the B.Sc. and M.Sc. degrees in electrical engineering from Xi'an Jiaotong University, Xi'an, China, in 2007 and 2010, respectively, and the Ph.D. degree from The Ohio State University, Columbus, OH, USA, in 2015.

She is currently an Assistant Professor with the Department of Electrical Engineering, University at Buffalo, Buffalo, NY, USA. Her research interests include dc arc detection, dc microgrid protection and control, and high-voltage dc transmission.

Vu Le (Student Member, IEEE) received the B.S. and M.S. degrees in electrical engineering, in 2016 and 2018, respectively, from the State University of New York at Buffalo, Buffalo, NY, USA, where he is currently working toward the Ph.D. degree in electrical engineering.

His current research interests include dc series arc fault detection, machine learning, field-programmable gate array implementation, and zonal protection.

Inhwan Lee (Member, IEEE) received the B.S. degree from Korea University, Seoul, South Korea, in 2014, and the Ph.D. degree from The State University of New York at Buffalo, Buffalo, NY, USA, in 2021, both in electrical engineering.

He is currently a Postdoctoral Research Associate with The State University of New York at Buffalo. His research interests include active gate drivers, wide-bandgap semiconductors, their series-connection technologies, modular multilevel converter, and high power electronics applications.